Coastal Engineering 58 (2011) 194–205

Contents lists available at ScienceDirect

Coastal Engineering

journal homepage: www.elsevier.com/locate/coastaleng

Assessment and integration of conventional, RTK-GPS and image-derived beach survey methods for daily to decadal coastal monitoring

Mitchell D. Harley [a,*], Ian L. Turner [a,1], Andrew D. Short [b], Roshanka Ranasinghe [c,d,e]

[a] Water Research Laboratory, School of Civil and Environmental Engineering, University of New South Wales, King Street, Manly Vale, NSW, 2093, Australia
[b] Coastal Studies Unit, School of Geosciences, University of Sydney, NSW 2006, Australia
[c] NSW Department of Environment, Climate Change and Water, Sydney, NSW, 2000, Australia
[d] Department of Civil Engineering and GeoSciences (CiTG), Delft University of Technology, PO Box 5048, 2600 GA Delft, The Netherlands
[e] Department of Water Engineering, UNESCO-IHE, PO Box 3015, 2601 DA Delft, The Netherlands

ARTICLE INFO

Article history:
Received 6 November 2009
Received in revised form 14 September 2010
Accepted 20 September 2010
Available online 23 October 2010

Keywords:
Beach surveys
Semivariogram
ARGUS coastal imaging
RTK-GPS
Collaroy–Narrabeen Beach

ABSTRACT

Coastal monitoring across a broad range of time-scales was recognized in the latest report by the Intergovernmental Panel on Climate Change as key to better understanding the likely impacts of climate change at the coast. A unique and historic coastal monitoring program undertaken at the Collaroy–Narrabeen embayment in south-eastern Australia comprises: 1) 30 years of monthly conventional (Emery method) surveys of five cross-shore profile lines; 2) three years of monthly three-dimensional surveys of the entire embayment using RTK-GPS mounted to an all-terrain vehicle (ATV); and 3) four years of hourly shoreline measurements using coastal imaging technology (ARGUS). This study evaluates the strengths and limitations of conventional, RTK-GPS and image-derived surveys for coastal monitoring at daily to decadal coastal time-scales. High-accuracy RTK-GPS was used to first assess the accuracy of the conventional and image-derived survey methods. The magnitude of daily to decadal coastal variability was then characterized by calculating the temporal semivariogram of the integrated survey dataset. With both measurement errors and the degree of beach variability quantified, the corresponding signal-to-noise ratios (SNR) of each survey method at different time-scales were determined. The value of the simple and cost-effective Emery method was verified by this analysis, with measurement error significantly smaller than the degree of overall beach variability (SNR = 8.4). The accuracy, speed and efficiency of ATV-mounted RTK-GPS meanwhile make it suitable for three-dimensional beach surveys. Image-derived surveys were found to be an effective means of remotely measuring the considerable degree of beach variability identified at time-scales of less than one month. These measurements however become indistinguishable from survey noise (i.e. SNR ≤ 1) when considering typical weekly (or smaller) variations at large distances from the cameras.

1. Introduction

Repeat surveys of the coastal zone provide great insight into the dynamics of coastal morphology. With specific regards to coastal engineering applications, survey data is a valuable resource for quantifying long-term recession and/or accretion trends (e.g. Nor-cross et al., 2002; Zhang et al., 2002), the degree of erosion and rate of recovery due to storm events (e.g. Sallenger et al., 1985; Egnese, 1989; Morton et al., 1994; List and Farris, 1999), the beach response to engineering works (e.g. Turner, 2006; Ojeda and Guillen, 2008), seasonal changes (e.g. Shepard, 1950; Fox and Davis, 1978; Masselink and Pattiaratchi, 2001) and interannual variability (e.g. Thom and Hall, 1991; Dingler and Reiss, 2002; Kroon et al., 2008).

Coastal monitoring was recognized in the latest report by the Intergovernmental Panel on Climate Change (Nicholls et al., 2007) as key to better understanding the likely impacts of climate change at the coast. Particularly, Nicholls et al. (2007) highlight that while the long-term (decade to century) implications of sea-level rise have been given considerable attention, more attention needs to be focussed on finer temporal and spatial scales, including the localized impacts of potential changes in wave climate and storminess regimes. However, coastal monitoring at this higher temporal (daily to decadal) and spatial (three-dimensional) resolution poses many challenges. Not only are ongoing beach surveys using conventional survey techniques both costly and labour-intensive, but also they typically require several years of data before meaningful trends emerge (Short and Trembanis, 2004). A comprehensive review of the literature (summarized in Table 1) consequently indicates very few multi-decadal, high-resolution coastal monitoring programs currently in operation worldwide.

* Corresponding author. Dipartimento di Scienze della Terra, Università di Ferrara, Via Saragat 1, 44100 Ferrara, Italy.
E-mail addresses: mitchell.harley@unife.it (M.D. Harley), ian.turner@unsw.edu.au (I.L. Turner), a.short@geosci.usyd.edu.au (A.D. Short), r.ranasinghe@unesco-ihe.org (R. Ranasinghe).
[1] Tel.: +61 2 80719800; fax: +61 2 99494188.

0378-3839/$ – see front matter.
doi:10.1016/j.coastaleng.2010.09.006

Table 1
List of coastal sites around the world with ongoing multi-decadal and high resolution coastal monitoring programs.

Site	Surveys undertaken	Example publications
Duck (USA)	Biweekly beach profiles (1981–present) ARGUS intertidal bathymetries (1986–present)	Lippmann and Holman (1990), Larson and Kraus (1994), Birkemeier et al. (1999)
Rhode Island (USA)	Monthly beach profiles (1962–present)	Lacey and Peck (1998)
Noordwijk (The Netherlands)	Annual beach profiles (1964–present) ARGUS intertidal bathymetries (1995–present) Monthly 3D dGPS (2001–2004)	Wijnberg and Terwindt (1995), Kroon et al. (2008), Quartel et al. (2008)
Lubiatowo (Poland)	Monthly beach profiles (1983–present)	Rozynski et al. (2001), Rozynski (2005)
Collaroy–Narrabeen (Australia)	Monthly beach profiles (1976–present) ARGUS intertidal bathymetries (2004–present) Monthly 3D RTK-GPS (2005–present)	Wright and Short (1984), Short and Trembanis (2004), Ranasinghe et al. (2004), Callaghan et al. (2008)
Moruya (Australia)	Monthly beach profiles (1972–present)	Thom and Hall (1991), McLean and Shen (2006)
Hasaki (Japan)	Daily beach profile (1987–present)	Kuriyama (2002), Kuriyama et al. (2008)

New survey technologies such as LiDAR (Light Detection And Ranging) and RTK-GPS (Real-Time Kinematic Global Positioning System) have facilitated analysis of spatial variability by allowing three-dimensional survey data to be collected both rapidly and at high spatial density. The advent of coastal imaging technology such as the ARGUS system (Holman and Stanley, 2007) addresses challenges of temporal variability. Using video cameras mounted on an elevated structure, high-frequency (typically hourly) beach survey data can be collected without the need to deploy *in situ* equipment or personnel. Furthermore, since these systems require relatively little cost or upkeep, they can be operating for many years.

The suitability of these survey datasets is however ultimately limited by their accuracy in relation to the degree of beach variability at the site. The signal-to-noise ratio (SNR) should be large enough to ensure that 'real' beach change signals dominate over the inherent random 'noise' due to measurement errors. For example, Sallenger et al. (2003) assessed the accuracy of LiDAR surveys of the USA's eastern coastline and concluded that the vertical error (approximately ±15 cm) did not impede the quantitative resolution of the large event-based changes for which LiDAR surveys were deployed. For higher-frequency survey programs such as those involving coastal imaging technology, careful attention needs to be given to the inherent measurement error in relation to the magnitude of beach variability at such short (i.e. daily to monthly) time-scales.

A unique coastal monitoring program undertaken at the Collaroy–Narrabeen embayment in southeast Australia combines three distinct beach survey techniques. Between 1976 and 2006, five cross-shore profile lines spaced along the subaerial beach (defined here as the section of the beach above mean sea level) were surveyed monthly using conventional (Emery method) survey techniques. This historic dataset has been used in previous studies to develop the morphodynamic beach state model of Wright and Short (1984), investigate embayed beach rotation and oscillation (Short and Trembanis, 2004; Ranasinghe et al., 2004) and to validate statistical modeling of coastline recession due to sea-level rise (Ranasinghe et al., 2009) and extreme beach erosion (Callaghan et al., 2008, 2009). Conventional surveys have since been replaced by two new survey schemes. Commencing in August 2004, hourly shoreline measurements have been undertaken using the coastal imaging (ARGUS). Monthly RTK-GPS surveys of both these five historical profile lines as well as three-dimensional surveys of the entire embayment have also been conducted since May 2005.

Prior to the introduction of these new surveys, the accuracy of the historical survey dataset had not been quantified. The limitations of coastal imaging technology – particularly its ability to accurately measure short-term shoreline variability at large distances from the cameras – also needed to be assessed. The aim of this study is to therefore evaluate the strengths and limitations of conventional, RTK-GPS and image-derived survey methods for daily to decadal coastal monitoring. A generic methodology is applied that first examines the error of the conventional and image-derived survey methods using the high-accuracy (approximately ±3 cm vertical) RTK-GPS measurements. Coastal variability from daily through to weekly, monthly, annually and decadal time-scales is then characterized by calculating the temporal semivariogram for this integrated dataset. The use of the temporal semivariogram is demonstrated to be an effective tool in determining the signal-to-noise ratio (and hence suitability) of each survey method across this broad range of time-scales.

2. Collaroy–Narrabeen beach survey program

2.1. Study site

The coastline of south-eastern Australia is microtidal, moderate to high wave energy and dominated by embayed beaches with an average length of 1 km (Short, 2007). The Collaroy–Narrabeen embayment is located within Sydney's northern beaches region of Sydney: around 20 km north of the tide gauge in Sydney Harbour (refer to Fig. 1). It is 3.6 km in length and is bounded at its southern end by Long Reef Point and at its northern end by Narrabeen Head. The beach is composed of fine to medium quartz sand ($D_{50} \approx 0.3$ mm), with approximately 30% carbonate fraction. Typical gradients for the intertidal and nearshore slope are 0.12 and 0.02 respectively.

The deepwater wave climate of the Sydney region consists of persistent southerly swell waves ($H_s \approx 1.6$ m, $T_p \approx 10$ s) interrupted approximately 5% of the time by storm waves exceeding 3 m (H_s) and reaching up to 8 m (Lord and Kulmar, 2000). The two headlands redistribute wave energy in the nearshore such that the northern (Narrabeen) end of the embayment is characteristically more exposed to the predominant southerly swell direction (Harley et al., 2007a).

2.2. Conventional surveys

The conventional survey program at Collaroy–Narrabeen was conducted between April 1976 and August 2006 by Professor Andrew Short and members of the Coastal Studies Unit, University of Sydney. Initially, nine cross-shore profile lines were surveyed at fortnightly intervals. Within a few years however, the survey program was altered to approximately monthly samplings (average interval = 33 days) of five representative profile lines, hereafter referred to as profile numbers 1, 2, 4, 6 and 8. These lines span the length of the embayment at an average alongshore spacing of 750 m (Fig. 1). A total of 335 surveys were performed using conventional survey techniques over this 30-year period.

Profile lines were measured using the Emery method (Emery, 1961), which is a low-cost technique requiring two people, each holding a survey rod (Fig. 2). Commencing with the landward rod on a fixed benchmark, the distance Δp_{conv} between the two rods is first measured using a measuring tape. The change in elevation Δz_{conv} between the two rods is then calculated by using the line-of-sight with the horizon and markings on the rods as a reference. This process is repeated at each subsequent measurement point along the entire

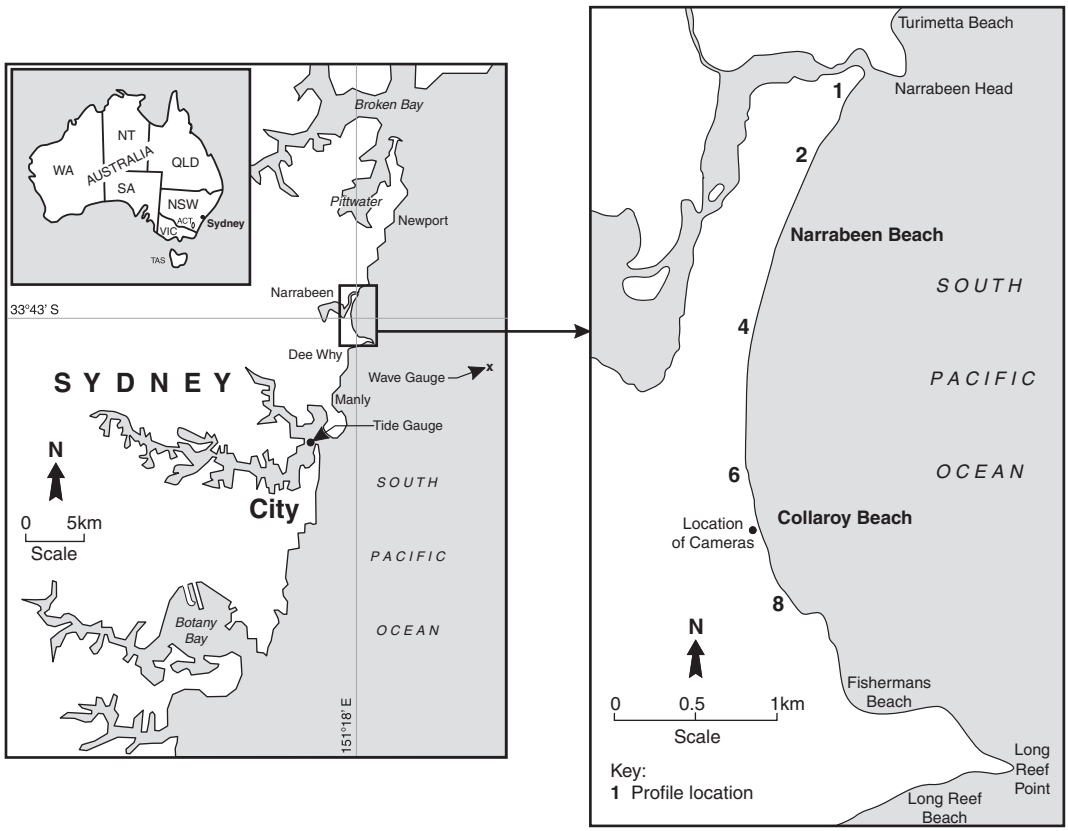

Fig. 1. The Collaroy–Narrabeen embayment on the south-east Australian coastline. Indicated are the locations of the five historical profile lines (referred to as profile numbers 1, 2, 4, 6 and 8) that have been surveyed approximately monthly since 1976.

length of the profile line. Since the elevation of the benchmark z_{BM} is known, relative (Δp_{conv} and Δz_{conv}) measurements can be converted to actual positions and elevations. A complete description of this technique is provided by Emery (1961). For the survey program at Collaroy–Narrabeen, readings were taken at fixed 10 m cross-shore intervals and continued until the profile intersected with MSL.

The simplicity of the Emery method meant that all five profile lines spread along the 3.6 km-long embayment could be surveyed within about an hour, which was a major contributing factor in maintaining the survey program for three decades. Conversely, the method's simplicity meant that it also had the potential to introduce significant measurement error. The sequential stepping procedure meant that the accuracy of each point was dependent upon the accuracy of all preceding points, such that vertical and cross-shore errors may accumulate. Additional uncertainty was also introduced by using linear interpolation to convert these 10 m cross-shore spaced points into a continuous profile line, particularly when a sharp break-in-slope was observed.

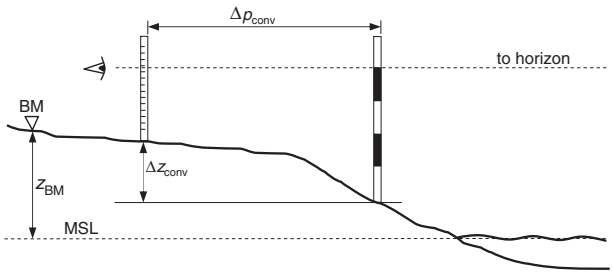

Fig. 2. The Emery method, which is used to measure the five profile lines. Cross-shore distances (Δp_{conv}) are measured using a measuring tape. Elevation changes are then calculated by using the line-of-sight with the horizon and markings on the rods as a reference. Knowing the benchmark elevation z_{BM}, these relative measurements are then converted to actual elevation values.

2.3. RTK-GPS surveys

RTK-GPS surveys commenced at Narrabeen in May 2005 using two approaches. First, measurements have continued on the five historical profile lines, though at an increased cross-shore resolution (approximately 0.5 m intervals). A total of 38 surveys of this type were completed up to August 2008 at an average survey interval of 32 days. Second, three-dimensional topographic surveys spanning the entire subaerial section (above MSL to a fixed boundary in the stable backbeach) of the beach have been performed each month. By mounting the RTK-GPS unit to an all-terrain vehicle (ATV), over 10 000 irregularly spaced points (x_{gps},y_{gps},z_{gps}) are collected per survey (Fig. 3a). The time to complete each survey is approximately 8 h. Measurement errors due to ATV sinking, tilting and shaking are observed to be within the accuracy of RTK-GPS (Harley et al., 2007b).

The curvature of the embayment makes the processing and analysis of this three-dimensional survey data difficult, particularly when trying to interpolate the irregularly spaced data to a fixed rectangular grid. This problem is overcome by transforming the irregular points (x_{gps}, y_{gps}, z_{gps}) within the curved embayment to alongshore (s) — cross-shore (p) coordinates (s_{gps}, p_{gps}, z_{gps}), using the method described by Harley and Turner (2008). Alongshore and cross-shore directions are defined relative to a logarithmic-spiral curve-fit of the embayment planform. In this new coordinate system the curvature of the embayment is effectively removed, making data interpolation considerably easier. For the surveys at Collaroy–Narrabeen, linear interpolation is used (grid resolution = 4 m alongshore × 1 m cross-shore). This regularly spaced digital terrain model (DTM) is then transformed back to real-world coordinates, also using

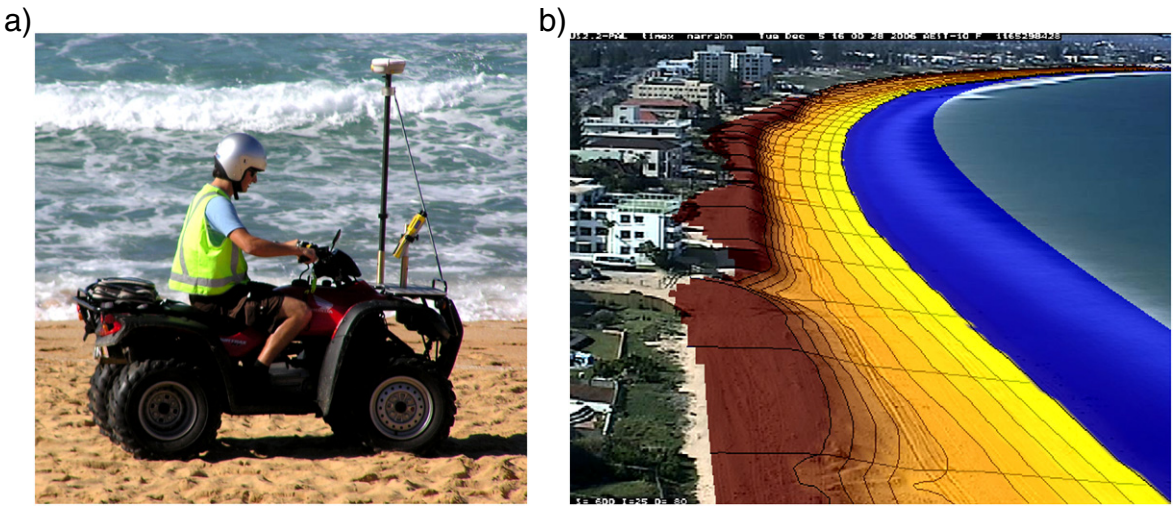

Fig. 3. Topographic surveying of the entire Collaroy–Narrabeen subaerial beach. a) Over 10 000 data points are collected using RTK-GPS mounted to an all-terrain vehicle (Photo: Brad Morris). b) These points are then interpolated to form a digital terrain model that resembles a dense (4 m alongshore spaced) series of cross-shore profile lines. A profile line only every 100 m is indicated for clarity.

the method of Harley and Turner (2008). Another advantage of this transformation method is that the format of the processed data resembles a series of densely spaced cross-shore profile lines (refer to Fig. 3b), which can be readily compared to the five historical transects. A total of 36 topographic surveys were completed up to August 2008.

2.4. Image-derived surveys

2.4.1. Collaroy–South Narrabeen station

In August 2004, an ARGUS coastal imaging station was installed at Collaroy–South Narrabeen to monitor high-frequency shoreline variability (including storm variability) not covered by the monthly *in situ* surveys (Turner et al., 2006). This station comprises five video cameras mounted on the roof of a beach-front apartment building (elevation = 44 m above MSL) and spans a 180° field of view of the southern half of the embayment (see Fig. 1). Only the southernmost (camera 1) and northernmost (camera 5) cameras are used in this study, which combine to cover an approximately 1300 m length of the embayment.

Every daylight hour, each camera collects the standard ARGUS suite of images: 1) single-frame 'snap' images; 2) 10-minute averaged 'timex' images; and 3) variance images of pixel intensities over 10 min (Holman and Stanley, 2007). In order to obtain quantitative information from these images, timex image coordinates (U_{image}, V_{image}) are rectified to real-world coordinates (x_{image}, y_{image}) using the method described by Holland et al. (1997). The plan-view shoreline position ($x_{sl,image}$, $y_{sl,image}$) is then located from these rectified images using the Pixel Intensity Clustering (PIC) technique (Aarninkhof et al., 2003).

Since manual use of the PIC technique is typically time-consuming and labour-intensive, an algorithm has been developed in collaboration with researchers from Deltares (The Netherlands) to apply the PIC technique automatically (Harley et al., 2007b; Uunk et al., 2010). This algorithm enables several thousands of shorelines to be processed retrospectively. As described by Uunk et al. (2010), careful quality-control of each shoreline is undertaken by this algorithm so that any falsely identified shoreline points (e.g. shadows on the beach, lines of wave breaking, etc.) are first discarded. Examples of timex images from cameras 1 and 5 overlaid with shorelines detected by the automated PIC technique are shown in Fig. 4.

2.4.2. Shoreline elevation model

Additional information is required to estimate the shoreline elevation z_{sl}. Several techniques have been adopted in the literature to estimate this elevation, such as an empirical modeling approach based on available field data (e.g. Davidson et al., 1997; Plant and Holman, 1997), a semi-empirical modeling approach based on field data combined with a one-line model of wave set-up through the surf zone (e.g. Aarninkhof et al., 2003; Plant et al., 2007), and a complete numerical modeling approach using two-dimensional hydrodynamic modeling (e.g. Siegle et al., 2007). Because of its transparency and the availability of extensive field data at Collaroy–Narrabeen (tide and offshore wave measurements), the empirical model approach was used for this study. As with other researchers who have used this method (Davidson et al., 1997; Aarninkhof et al., 2003; Plant et al., 2007; Ojeda and Guillen, 2008), a constant alongshore elevation Z_{sl} was assumed.

As a first pass, $Z_{sl,model}$ was estimated as a function of tidal variations alone. This is given by:

$$Z_{sl,model} = \alpha_0 + \alpha_{tide} Z_{tide} \quad (1)$$

where Z_{tide} is the measured tidal elevation, α_{tide} is an empirically derived coefficient that takes into account any tidal-modulation of Z_{sl}, and α_0 is an empirically derived constant vertical offset due to both wave run-up/set-up processes and differences between the actual and detected shoreline.

Previous research has found that wave run-up and set-up at the shoreline is proportional to $\sqrt{H_0 L_0}$ (Komar, 1998), where H_0 is the offshore significant wave height and L_0 is the offshore wave length computed from linear wave theory:

$$L_0 = \frac{gT_p^2}{2\pi} \quad (2)$$

Nielsen (1988) and Nielsen and Hanslow (1991) confirmed this relationship using extensive field data from Dee Why Beach, an embayment both immediately adjacent to and morphologically similar to that of Collaroy–Narrabeen. Hence in order to incorporate the additional effects of wave run-up/set-up variations due to changes in wave energy, the linear model in Eq. (1) becomes:

$$Z_{sl,model} = \beta_0 + \beta_{tide} Z_{tide} + \beta_{wave} \sqrt{H_0 L_0} \quad (3)$$

where β_{tide} and β_{wave} are empirically derived coefficients and β_0 is the empirically derived constant vertical offset between the detected and actual shoreline. The elevation model parameters for the simple tidal

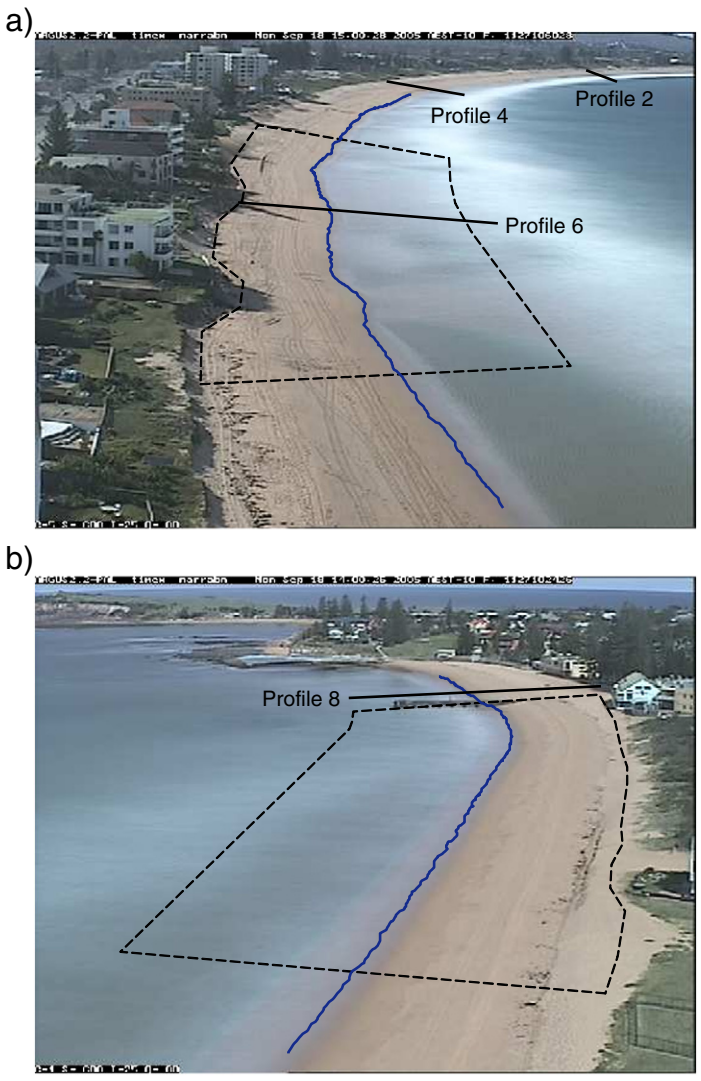

Fig. 4. Timex images from the Collaroy–South Narrabeen cameras: a) Camera 5 (pointing northwards); and b) Camera 1 (pointing southwards). Shorelines (blue lines) mapped on rectified versions of these images by the automated PIC technique are indicated. Dashed lines represent the areas used to calibrate the shoreline elevation models.

model (α_0 and α_{tide} in Eq. (1)) and the tide and wave model (β_0, β_{tide} and β_{wave} in Eq. (3)) are determined in the following section. Wave measurements were obtained from the Sydney waverider buoy, located 11 km offshore of Collaroy–Narrabeen in approximately 80 m water depth. Tide measurements were obtained from a tide gauge at the entrance to nearby Sydney Harbour (for the locations of both, refer to Fig. 1).

3. Accuracy of survey methods

3.1. Accuracy of conventional surveys

The accuracy of the conventional survey dataset was assessed using 16 surveys (i.e. 80 profile lines) between May 2005 and August 2006 when all five historical profile lines were measured concurrently by both the Emery method and high-accuracy RTK-GPS. During each of these 16 surveys, the height and position of each individual Emery method measurement were also recorded by RTK-GPS (425 concurrent measurements in total). This enabled the error associated with each individual step of the Emery method (i.e. measurement of Δp_{conv}, and Δz_{conv}) to be explicitly quantified. Benchmark elevations z_{BM} were also measured by RTK-GPS and compared to previously assumed values. The comparisons identified discrepancies in benchmark elevations of up to 0.7 m. These systematic offsets were subtracted from the conventional survey data prior to further analysis.

Fig. 5 summarizes results of deviations between RTK-GPS and conventional measurements (defined as RTK-GPS minus conventional survey measurements). Vertical deviations due to the Δz_{conv} measurements have a mean and standard deviation of 0.02 m and 0.04 m respectively (Fig. 5a). Likewise, horizontal deviations due to the Δp_{conv} measurements have a mean and standard deviation of −0.14 m and 0.26 m respectively (Fig. 5b). These results suggest that Δz_{conv} values are slightly under-estimated on average by the conventional survey method, whereas Δp_{conv} values are slightly over-estimated.

The combined effect of Δz_{conv} and Δp_{conv} errors and their accumulation along each profile line are shown in Fig. 5c. Fortuitously, the seaward beach slope means that accumulation effects due to the previous biases are minimised. Hence there is no obvious offset when combining the two effects (mean vertical deviation = −0.04 m and standard deviation = 0.11 m).

Comparing the complete profile lines derived from the two survey methods (i.e. including the additional uncertainty in linearly interpolating the 10 m-spaced conventional survey points to form a complete profile line) results in approximately normally distributed vertical deviations with a mean of −0.03 m and a standard deviation

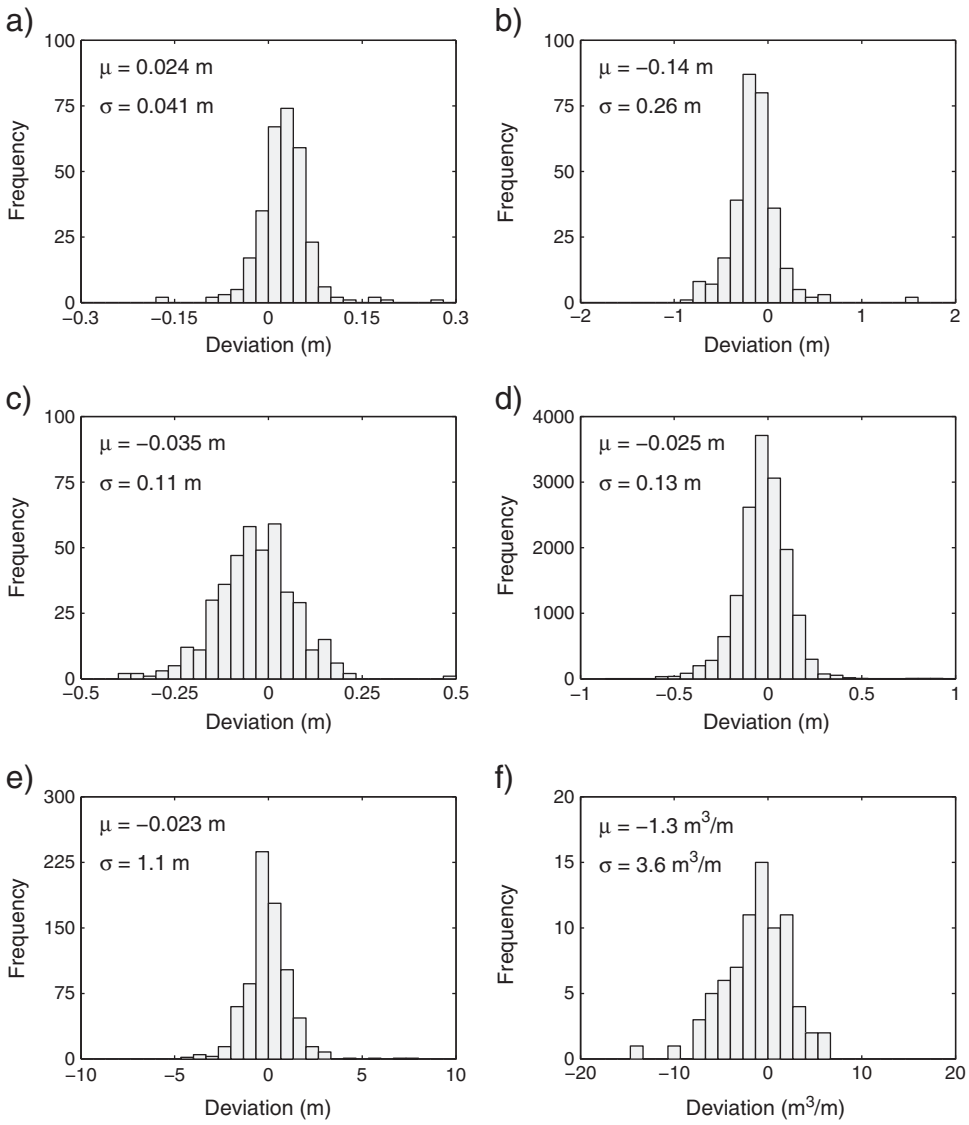

Fig. 5. Frequency distributions of deviations between RTK-GPS and conventional (Emery method) survey measurements: a) vertical deviations due to change in elevation (Δz_{conv}) measurements; b) horizontal deviations due to cross-shore distance (Δp_{conv}) measurements; c) vertical deviations due to combined Δz_{conv} and Δp_{conv} measurements d) overall vertical profile deviations; e) cross-shore profile deviations in the intertidal zone; and f) deviations in the subaerial volume calculation.

of 0.13 m (Fig. 5d). In the intertidal zone (between MSL and +2 m), this translates to a cross-shore standard deviation of 1.1 m (Fig. 5e).

Finally, the subaerial volume calculations (defined as the volume per meter of beach above the 0 m contour) derived from each survey method were compared (Fig. 5f). These deviations were found to have a mean of −1.3 m^3/m and a standard deviation of 3.6 m^3/m.

3.2. Accuracy of image-derived surveys

A total of 307 automated shorelines were processed from timex images at cameras 1 and 5 (refer to Table 2) to first calibrate the elevation model parameters in Eqs. (1) and (3). These shorelines were collected over 16 topographic survey days between July 2005 and December 2006. Actual shoreline elevations $z_{sl,gps}$ were calculated by interpolating image shoreline locations ($x_{sl,image}$, $y_{sl,image}$) to the RTK-GPS DTM. These values were then averaged alongshore to obtain a single shoreline elevation $Z_{sl,gps}$. In order to avoid biasing by shoreline outliers (i.e. in the far-field of each image), only shoreline data within approximately 400 m alongshore regions (shown in Fig. 4) where the shoreline-detection technique was observed to perform most consistently were considered.

Table 2
Statistics of environmental conditions during image-derived shoreline calibrations. Intertidal slopes were based on RTK-GPS topographic survey measurements between MSL and +2 m at the southern end of the embayment.

Date	Shorelines mapped		H_s (m)	T_p (s)	Dir (°)	Intertidal slope
	Camera 1	Camera 5				
22/07/05	11	8	1.2	12.6	155	0.13
21/08/05	11	7	1.2	8.6	161	0.16
19/09/05	10	10	1.6	9.4	109	0.15
18/10/05	10	11	2.3	7.7	109	0.11
17/11/05	13	12	2.3	9.2	142	0.12
05/12/05	4	4	1.0	8.8	154	0.14
15/12/05	11	11	1.1	8.8	133	0.15
30/01/06	7	9	1.0	9.3	98	0.11
12/04/06	12	12	1.0	6.2	45	0.10
23/05/06	9	9	2.5	8.7	179	0.10
27/06/06	10	8	1.2	8.5	165	0.10
28/07/06	9	8	2.3	10.4	73	0.13
13/09/06	11	10	1.6	10.4	146	0.12
11/10/06	10	9	2.0	12.9	96	0.11
06/11/06	11	10	2.7	8.7	150	0.12
05/12/06	10	10	0.9	12.4	178	0.12
Total/mean	159	148	1.6	9.5	133	0.12

Fig. 6a shows the alongshore-averaged shoreline elevations $Z_{sl,gps}$ compared to tidal levels Z_{tide}. Using linear regression, the best-fit parameters (at a 95% confidence level) are $\alpha_0 = 0.72\ m \pm 0.02\ m$ and $\alpha_{tide} = 1.20 \pm 0.04$ ($R^2 = 0.91$). The root mean square (RMS) error is 0.19 m.

The additional effects of wave set-up and run-up variations due to wave energy changes were explored by comparing daily averaged residuals ΔZ_{res} from the previous linear models ($\Delta Z_{res} = Z_{sl,gps} - \alpha_{tide} Z_{tide}$) to daily averaged values of $\sqrt{H_0 L_0}$. As highlighted in Fig. 7, these two variables are significantly correlated ($R = 0.79$ and $p < 0.001$). This suggests that including the $\sqrt{H_0 L_0}$ term in the elevation model would improve the overall accuracy of the image-derived shorelines. Multiple linear regression was used to find the parameters for the tide and wave elevation model in Eq. (3). The best-fit parameters (at a 95% confidence level) are $\beta_0 = 0.31\ m \pm 0.07\ m$, $\beta_{tide} = 1.22 \pm 0.04$ and $\beta_{wave} = 0.03 \pm 0.005$ ($R^2 = 0.94$). The resulting RMS error is now 0.15 m, a 20% improvement on the tide-only model (Fig. 6b).

To evaluate the vertical and cross-shore accuracy along the entire 1300 m survey region of the two cameras, the 307 image-derived shorelines with coordinates ($x_{sl,image}, y_{sl,image}, Z_{sl,model}$) were transformed to alongshore–cross-shore coordinates ($s_{sl,image}$, $p_{sl,image}$, $Z_{sl,model}$), again using the method of Harley and Turner (2008). Vertical deviations from RTK-GPS measurements are shown in Fig. 8a. Since the intertidal beach slope is roughly uniform in this region, cross-shore deviations are approximately proportional to vertical deviations (Fig. 8b). Positive values in these figures can be interpreted as either an under-estimation of the shoreline elevation, or a more landward detection of the shoreline position at these locations.

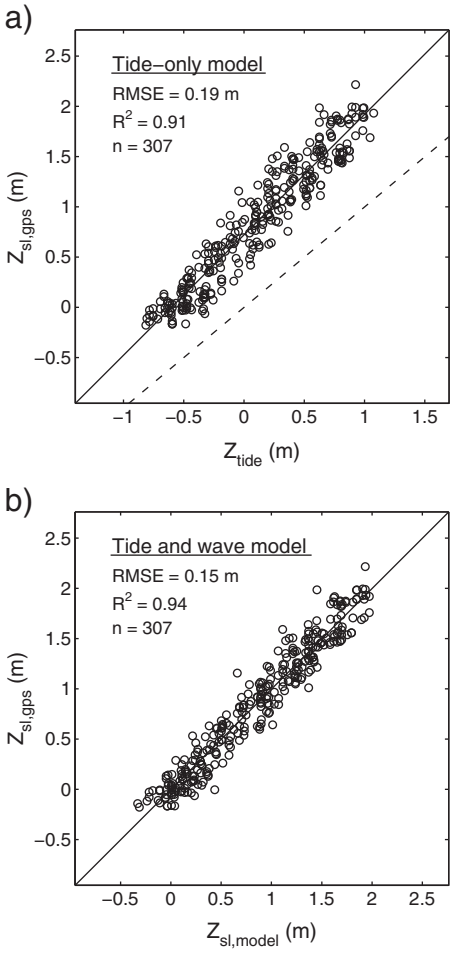

Fig. 6. Calibration of the elevation models for the Collaroy–South Narrabeen cameras: a) alongshore-averaged measured shoreline elevations $Z_{sl,gps}$ versus tidal levels Z_{tide}. The dashed line represents a 1:1 ratio. b) $Z_{sl,gps}$ versus the modeled shoreline elevations $Z_{sl,model}$ using the tide and wave elevation model in Eq. (3).

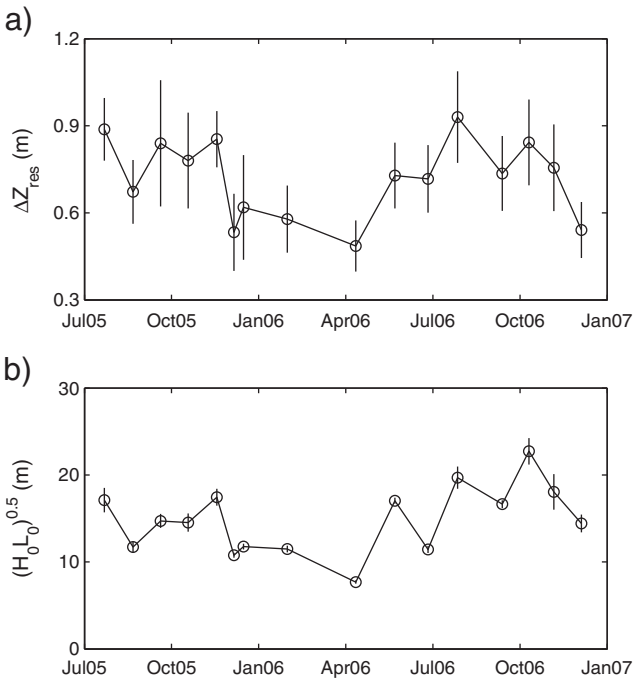

Fig. 7. Daily averaged values of elevation residuals ΔZ_{res} from the tide-only elevation model over the validation period; and b) daily averaged values of over the validation period. Vertical bars represent ± one standard deviation.

Considering the more accurate tide and wave elevation model (i.e. Eq. (3)), 85% of the mean deviations of measured shorelines in this region are less than 0.15 m (vertical) and 1.0 m (cross-shore, horizontal). Shoreline measurements are most accurate in the near-field (approximately 150 m alongshore from the cameras) and diminish as the image resolution decreases with distance from the cameras. The minimum standard deviation of vertical (cross-shore) deviations is 0.15 m (1.2 m) in the near-field of camera 1 and the maximum is 0.44 m (4.1 m) in the far-field of camera 5 (approximately 1000 m alongshore from the camera). Overall, 50% of the 1300 m region has a standard deviation less than 0.20 m (vertical) and 1.7 m (horizontal) and 85% less than 0.30 m (2.6 m).

4. Assessment of survey accuracy in relation to beach variability

Having evaluated the accuracy of both the conventional and image-derived survey methods, this section demonstrates a generic methodology to place these values into the context of observed beach variability. This assessment was performed over a range of time-scales by combining high-frequency image-derived survey data with the long-term conventional/RTK-GPS profile data. Beach variability is described here by the cross-shore variability in shoreline position — the only variable explicitly quantified by all three survey methods. Specifically, the shoreline position is defined by the mean high-water springs (MHWS, approximately 0.7 m above MSL) contour line. This position is represented in cross-shore coordinates (i.e. relative to the logarithmic-spiral curve-fit of the beach planform) and is hereafter referred to as p_{mhws}.

Time-series of p_{mhws} between April 1976 and August 2008 were constructed from the combined conventional/RTK-GPS profile data at the five profile locations. As a comparison, these time-series were cross-correlated with time-series of other standard beach variability parameters, such as the 0 m/2 m contour lines and subaerial beach

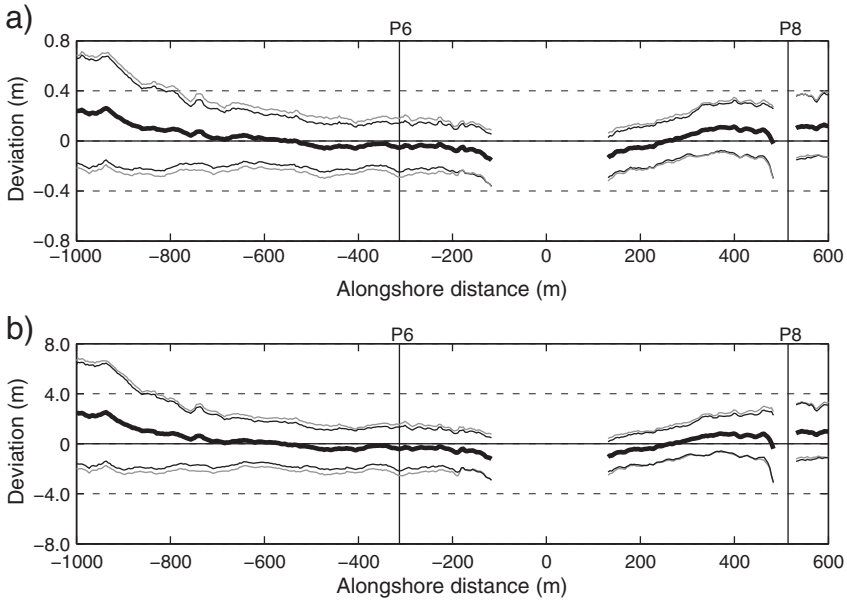

Fig. 8. a) Vertical, and b) cross-shore standard deviations of image-derived shoreline measurements from RTK-GPS measurements at the Collaroy–South Narrabeen station. Thin grey lines are from the tide-only model and thin black lines from the more accurate tide and wave elevation model. The thick black line represents the mean deviation. Alongshore distances represent the distance southwards from the camera station.

volume. The results (summarized in Table 3) indicate that these three parameters are strongly correlated (R>0.9) to p_{mhws}.

4.1. Magnitude of shoreline variability: 1976–2008

Statistics of cross-shore shoreline variability p_{mhws} between 1976 and 2008 at the five profile locations are indicated in Table 4. Variability over this 32-year period is greatest at Profiles 1 and 4 (standard deviation = 14 m, range = 79 m and 73 m respectively) and least at Profile 6 (standard deviation = 9.2 m, range = 54 m).

Analysis of the magnitude of shoreline variability across a range of time-scales was confined to data at Profile 6, which is the only profile line located within a reasonable distance of the cameras (see Fig. 4). A total of 7620 shorelines at various elevations were collected using the automated PIC technique on rectified timex images between August 2004 and August 2008. From this set of shorelines, 1145 daily measurements of p_{mhws} at Profile 6 were obtained using the quadratic loess interpolation method of Plant et al. (2002). This interpolation method smooths any small-scale variability due to shoreline-detection errors.

Fig. 9a shows p_{mhws} at Profile 6 between 1976 and 2008 from both monthly conventional/RTK-GPS and daily image-derived data. For clarity, a three-day smoothing window was applied to the time-series of image-derived p_{mhws} values using a forward–backward zero-phase filter. During this period, p_{mhws} varies between a minimum of 25 m in June 1980 and a maximum of 79 m in April 1982. No significant net accretion or erosion trends are apparent at this location and the shoreline can be seen to vary around the mean of 45 m. Short and Trembanis (2004) and Ranasinghe et al. (2004) found that this variability is indicative of interannual cycles of beach oscillation and rotation within the embayment.

Fig. 9b indicates p_{mhws} at Profile 6 between 2005 and 2007 when concurrent surveying using all three techniques occurred. This plot highlights the degree of intra-annual variability, particularly in response to individual and sequential storm events. In this two-year period, p_{mhws} ranges between a minimum of 30 m in July 2005 and a maximum of 65 m in March 2006. As much as 25 m of shoreline recession in only 8 days was observed due to a storm event in May 2005 (refer to wave heights in Fig. 9c). A series of storm events in July 2006 also resulted in 21 m of recession over 17 days.

4.2. Semivariogram and signal-to-noise ratio analysis

Visual inspection of Fig. 9b suggests that the conventional and image-derived survey methods adequately capture the dominant beach cycles and trends identified over this two-year period. Semivariogram analysis was used as a more rigorous means of characterizing the magnitudes of shoreline variability from daily to decadal time-scales. The empirical semivariogram estimates typical magnitude of change between two points at a spatial or temporal lag h. It has previously been applied in beach studies as a means of characterizing the spatial variability of survey data (e.g. Phillips, 1986; Dolan and Davis, 1992; Mason et al., 1997; Swales, 2002). For a time-series of cross-shore shoreline position $p_{mhws}(t)$, the empirical

Table 3
Correlation coefficients between time-series of the cross-shore shoreline position at mean high water springs (p_{mhws}) and: 1) mean sea level (p_{msl}); 2) the 2 m elevation (p_{+2}); and 3) subaerial volume above MSL. Data is based on monthly conventional/RTK-GPS surveys at the five historical profile lines between 1976 and 2008.

Profile number	1	2	4	6	8
MSL position p_{msl}	0.97	0.95	0.99	0.97	0.97
+2 m position p_{+2}	0.92	0.90	0.90	0.94	0.90
Subaerial volume (above MSL)	0.91	0.90	0.93	0.94	0.96

Table 4
Statistics of cross-shore shoreline position (p_{mhws}) at the five profile locations, based on monthly conventional/RTK-GPS surveys between 1976 and 2008.

Profile number	1	2	4	6	8
Mean (m)	48	44	51	45	41
Std. dev.	14	11	14	9.2	12
Min. (m)	18	13	17	25	15
Max. (m)	97	81	90	79	78
Range (m)	79	68	73	54	64
Linear trend (m/year)	0.13 ±0.14	0.22 ±0.11	−0.50 ±0.12	0.06 ±0.10	−0.28 ±0.12

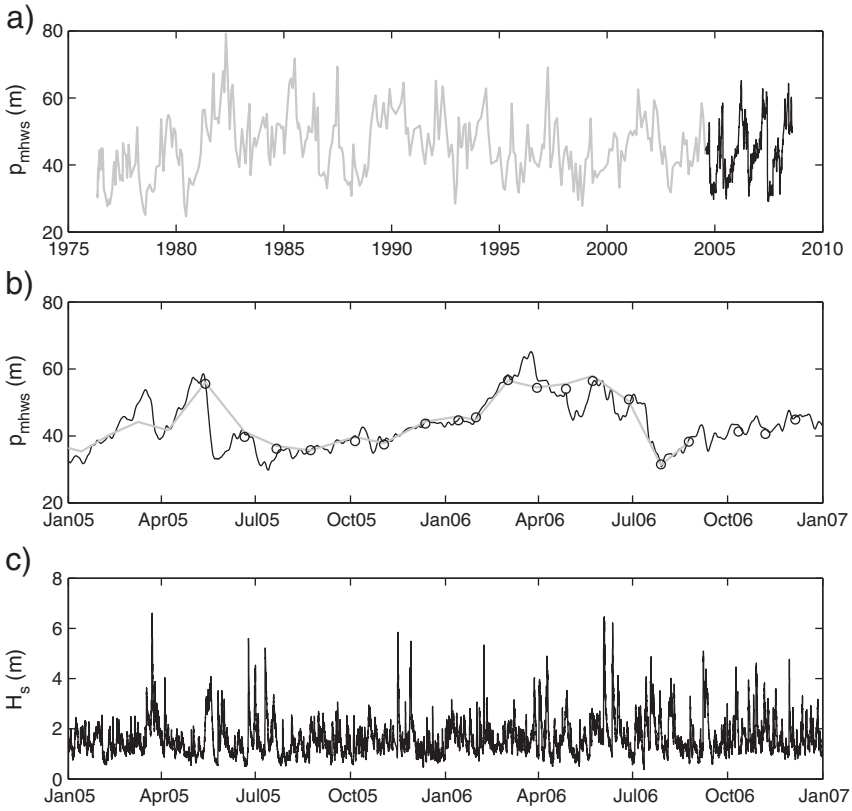

Fig. 9. a) Time-series of MHWS shoreline position p_{mhws} at Profile 6 between 1976 and 2008 from conventional (grey line) and image-derived (black line) surveys. b) Close up of the period from 2005 to 2007 when concurrent surveying using conventional, image-derived and RTK-GPS (black circles) methods occurred. c) Significant wave height collected from the Sydney waverider buoy over this two-year period.

semivariance (in units of m^2) at a temporal lag (i.e. time-scale) h is given by:

$$\hat{\gamma}(h) = \frac{1}{2N(h)} \sum_{i=1}^{N(h)} \left[(p_{mhws}(t+h) - p_{mwhs}(t))_i \right]^2 \quad (4)$$

where $N(h)$ denotes the number of data pairs at lag h. Although theoretically the semivariogram is equal to zero at $h=0$, any noise due to measurement error and micro-scale variability means that in practice this value is typically greater than zero. At longer lags, the semivariogram theoretically asymptotes towards the overall variance ($\sigma^2_{overall}$) at a point known as the 'range'. This value can be interpreted as the distance or time-scale where any dependence between a pair of data points is lost (Davis, 2002).

The empirical semivariogram was calculated for the combined (image-derived and conventional/RTK-GPS) 32-year shoreline position time-series depicted in Fig. 9a. Semivariance at daily to monthly time-scales was calculated from 1145 daily image-derived shoreline positions, while 357 monthly conventional/RTK-GPS shoreline positions were used to calculate the semivariance at monthly to decadal time-scales.

The empirical semivariogram, converted to units of meters ($\sqrt{\hat{\gamma}(h)}$), is plotted in Fig. 10. $\sqrt{\hat{\gamma}(h)}$ is shown to asymptote towards the overall variability (in this case, the standard deviation of shoreline position at Profile 6) at a range (i.e. time-scale) of approximately 15 months. Fluctuations between yearly and decadal lags around this overall value are indicative of beach rotation and oscillation processes at this profile line, which occur at similar time-scales (Short and Trembanis, 2004; Ranasinghe et al., 2004). As lags become shorter, the magnitude of typical shoreline variability is also observed to decrease. The fact that this decrease occurs quite rapidly is representative of the large degree high-frequency shoreline variability depicted in Fig. 9b. The magnitude of typical shoreline variability at one month time-scales is estimated from the semivariogram as 5.6 m, or of the order of 60% of the overall standard deviation. Notably there is a smooth transition between image-derived data and conventional survey data, with a similar semivariance at one month calculated from both datasets. At weekly time-scales, typical variability (3.1 m) is still relatively high, equivalent to 33% of the overall standard deviation.

To visualise the signal-to-noise ratio, the standard deviation of cross-shore error obtained in Section 2.2 for both the conventional ($\sigma_{signal} = 1.1$ m) and image-derived ($\sigma_{noise} = 1.7$ m for 50% of the 1300 m survey region at the southern end of the beach) survey data is plotted in Fig. 10. Trenberth (1984) defines the SNR as the ratio of standard deviations σ, given by the equation:

$$SNR = \frac{\sigma_{signal}}{\sigma_{noise}} \quad (5)$$

Applying this definition, the overall SNR of the conventional and image-derived datasets at Profile 6 is 8.4 and 5.4 respectively ($\sigma_{signal} = 9.2$ m) and decreases to 5.1 and 3.3 respectively when considering typical variability at monthly time-scales ($\sigma_{signal} = 5.6$ m). Fig. 9b suggests that these values are sufficient in capturing the beach cycles and patterns identified over this two-year period. The ability of the image-derived survey method to adequately monitor typical variability at finer temporal scales (weekly) however is dependent on the distance from the cameras. For instance, typical beach variability at a weekly time-scale ($\sigma_{signal} = 3.1$ m) is almost three times greater than the survey error in the near-field (approximately 150 m alongshore from the cameras) of camera 1 ($\sigma_{noise} = 1.2$ m), whereas in the far-field (approximately 1000 m alongshore from the cameras) of camera 5 survey error dominates ($\sigma_{noise} = 4.1$ m). Typical variability in this region is therefore indistinguishable from survey noise (i.e. SNR ≤ 1), which restricts the monitoring of

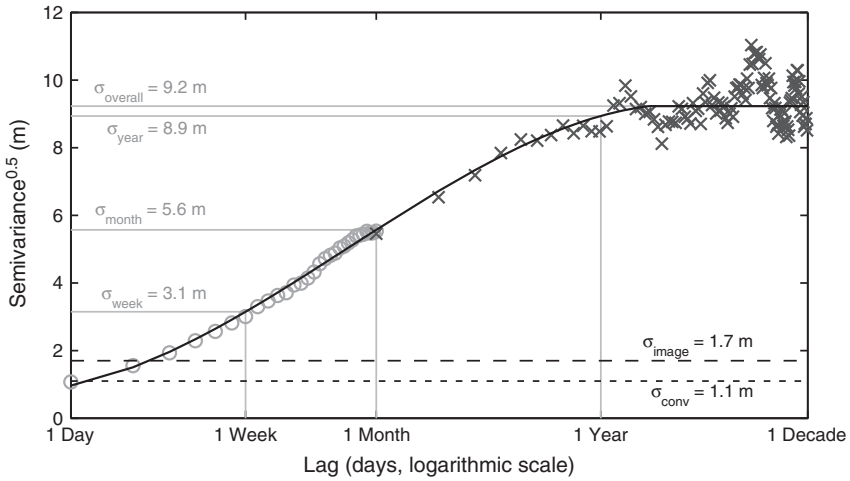

Fig. 10. The empirical semivariogram (converted to units of meters) for Profile 6, which is used to characterize typical cross-shore shoreline (p_{mhws}) variability at different time-scales. Image-derived shoreline data (circles) were used for daily to monthly lags, while conventional shoreline data (crosses) were used for monthly to decadal lags. The solid line is a smooth fit across the two datasets.

typical beach change at weekly time-scales to the near-field. This does not suggest that data in the far-field of images should be rejected outright. For large events such as the 25 m of storm recession observed in Fig. 9b, the SNR in the far-field is large enough (SNR = 6.1 for this particular event) for storm signals to be detected.

5. Discussion

With the absence of a single beach survey technology capable of measuring the broad range of spatial and temporal scales relevant to coastal engineering applications: this study has demonstrated the successful implementation of a coastal monitoring program using a combination of survey technologies. Each survey technique has unique advantages that make them suited to particular monitoring situations. The Emery method has been shown to be a reliable and cost-effective means of obtaining long-term two-dimensional beach profile information, with only a slight reduction in survey accuracy found in comparison to more sophisticated techniques. High-accuracy RTK-GPS technology mounted to an ATV enables the entire three-dimensional subaerial beach to be measured at dense spatial scales without the significant costs associated with, for example, ongoing LiDAR surveys. Coastal imaging technology further contributes by enabling high-frequency shoreline information (such as the beach response to individual storm events) to be measured in either real-time or retrospectively.

The successful application and integration of these survey techniques is primarily attributed to the highly dynamic nature of this embayed beach system. Both Collaroy and Narrabeen beaches are intermediate beach systems according to the morphodynamic beach state model of Wright and Short (1984). The beach therefore perpetually undergoes significant morphological modifications in response to its highly variable wave climate. At more stable sites (such as reflective and dissipative beach systems), a smaller beach signal – and hence SNR – might be expected (Wright and Short, 1984). At the same time however, such high-frequency monitoring may not be required at these sites.

Coastal imaging technology is particularly attractive to coastal managers because of its ability to collect data remotely and at relatively low cost. Furthermore, as performed in this study, image-derived shorelines can be collected automatically with very little user-input required. The degree of accuracy attained by image-derived surveys however appears to be somewhat site-specific. Plant et al. (2007) evaluated the performance of image-derived shorelines at various sites and reported vertical RMS errors in the range of 0.1 m to 0.4 m. The comprehensive evaluation undertaken here at the Collaroy–Narrabeen embayment found errors in the lower limit of this range (RMS error = 0.15 m), indicating that this site has one of the more successful examples of image-derived surveying demonstrated in the literature to date. Aside from the large amount of data available at this site for improved shoreline calibrations, this higher accuracy is likely the result of several advantageous site-specific factors: the relatively strong colour contrast between sand and water; the steepness of the beach face (and subsequently narrow swash zone); the clear and sunny conditions that typically prevail; and the relatively high viewing angle and close proximity of the ARGUS cameras. All these factors combine to produce an easily discernable shoreline at a high pixel resolution.

The model used to calculate the shoreline elevation also varies from site to site. Plant et al. (2007) utilized the semi-empirical modeling approach of Aarninkhof et al. (2003) for estimating the shoreline elevation, which requires calibration of a wave run-up coefficient k_{osc}. The present study however used a simple empirical elevation model based on measured tide and wave data only. Overall, tidal-modulation of the shoreline elevation was found to be the dominant process, accounting for over 90% of the variability in Z_{sl}. Significantly, since $\alpha_{tide} = 1.20$ and $\beta_{tide} = 1.22$ (i.e. greater than one), the vertical offset between shoreline elevation Z_{sl} and tide level Z_{tide} is greater at high tide (offset ≈ 0.9 m) than at low tide (offset ≈ 0.6 m). This is most likely due to the surf zone becoming increasingly saturated at low tide at this site, as wave energy dissipates over the prevailing sand bar (Wright and Short, 1984). Tidal-modulation of the vertical offset between Z_{sl} and Z_{tide} is unaccounted for in the semi-empirical elevation modeling approach, which effectively assumes $\beta_{tide} = 1.00$. This may be a consequence of the majority of sites tested using this approach (Plant et al., 2007) being less energetic and having a flatter beach face than the Collaroy–Narrabeen site, making tidal-modulation effects less distinguishable. Since it is desirable to implement coastal imaging surveys in the future without the need for on-site calibrations, further understanding of how β_{tide} varies with beach conditions is necessary.

6. Conclusion

This study has rigorously and quantitatively evaluated 30 years of conventional profile line surveys with four years of hourly image-derived shoreline measurements and three years of three-dimensional RTK-GPS surveys at the Collaroy–Narrabeen embayment, Australia. Using the high-accuracy of RTK-GPS as the control dataset, errors in the

conventional and image-derived surveys were assessed. Vertical deviations between the conventional and RTK-GPS profile lines were shown to be approximately normally distributed (i.e., 'random') with a standard deviation of 0.13 m (or 1.1 m in the horizontal, cross-shore direction). Image-derived shorelines have a comparable level of accuracy to the conventional surveys, with 50% of the 1300 m survey region having a vertical standard deviation less than 0.2 m (1.7 m for cross-shore deviations). The accuracy also varies significantly alongshore, being at a minimum in the camera near-field (vertical standard deviation = 0.15 m at approximately 150 m alongshore distance from the cameras) and maximum in the camera far-field (vertical standard deviation = 0.44 m at approximately 1000 m alongshore distance from the cameras).

In comparison to the degree of beach variability at the site, results indicate that survey errors have minimal impact on data analysis. The standard deviation of cross-shore shoreline position observed through the 32-year survey program was found to be 9.2 m for Profile 6 and up to 14 m for Profiles 1 and 4. Hence the 'signal' of shoreline variability is shown to be almost an order of magnitude larger than the 'noise' associated with measurement errors. Semivariogram analysis of the data highlights the large degree of beach variability at finer time-scales. At time-scales of one week, the typical variability of the data is one-third of the typical variability over the entire 32 years. Shoreline recessions of up to 25 m are also observed over the course of a single storm event.

The main differences between survey methods found in this study are primarily practical considerations with regards to the spatial and temporal scales of interest. By measuring the beach remotely and automatically, image-derived surveys are particularly effective at capturing high-frequency beach variability without the effort and costs associated with equivalent *in situ* techniques. The high-accuracy, speed and efficiency of the ATV-mounted RTK-GPS meanwhile make it suited to three-dimensional beach surveys. Finally, conventional surveys have been shown to be a simple and cost-effective way of obtaining longer-term survey data with only slight reductions in survey accuracy compared to more sophisticated techniques.

Acknowledgements

This study was supported by the Australian Research Council (grant # LP0455157), NSW Department of Environment, Climate Change and Water, Warringah Council and Deltares. The wave and tide data were kindly supplied by the Manly Hydraulics Laboratory on behalf of the NSW Department of Environment, Climate Change and Water. MDH would like to thank Stefan Aarninkhof, Robin Morelisson and Antonio Cerezo at Deltares for their assistance with the development and application of the ARGUS software; and all authors acknowledge Rob Holman and the team at the Coastal Imaging Lab (Oregon State University) for their role in developing and supporting the ARGUS program over many years. The comments of the anonymous reviewer also improved the manuscript considerably. MDH was funded by an APA (Industry) scholarship. Finally, the authors would like to thank the many people who have assisted in the collection of the Collaroy–Narrabeen dataset over the last 30+ years.

References

Aarninkhof, S.G.J., Turner, I.L., Dronkers, T.D.T., Caljouw, M., Nipius, L., 2003. A video-based technique for mapping intertidal beach bathymetry. Coastal Engineering 49, 275–289.

Birkemeier, W.A., Nicholls, R.J., Lee, G., 1999. Storms, storm groups and nearshore morphologic change. In: Kraus, N.C., McDougal, W. (Eds.), Coastal Sediments '99, vol. 2. ASCE, Long Island, U.S.A, pp. 1109–1122.

Callaghan, D.P., Nielsen, P., Short, A., Ranasinghe, R., 2008. Statistical simulation of wave climate and extreme beach erosion. Coastal Engineering 55, 375–390.

Callaghan, D.P., Ranasinghe, R., Short, A., 2009. Quantifying the storm erosion hazard for coastal planning. Coastal Engineering 56, 90–93.

Davidson, M., Huntley, D., Holman, R., George, K., 1997. The evaluation of large scale (km) intertidal beach morphology on a macrotidal beach using video images. In: Thornton, E.B. (Ed.), Coastal Dynamics '97, vol. 1. ASCE, Plymouth, U.K., pp. 385–394.

Davis, J.C., 2002. Statistics and data analysis in geology, 3rd ed. John Wiley and Sons.

Dingler, J.R., Reiss, T.E., 2002. Changes to Monterey Bay beaches from the end of the 1982-83 El Nino through the 1997–98 El Nino. Marine Geology 181 (1–3), 249–263.

Dolan, R., Davis, R.E., 1992. An intensity scale for atlantic coast northeast storms. Journal of Coastal Research 8 (4), 840–853.

Egnese, A., 1989. Southern California beach changes in response to extraordinary storm. Shore and Beach 57 (4), 14–17.

Emery, K.O., 1961. A simple method of measuring beach profiles. Limnology and Oceanography 6 (1), 90–93.

Fox, W.T., Davis, R.A., 1978. Seasonal variation in beach erosion and sedimentation on the Oregon coast. Geological Society of America Bulletin 89 (10), 1541–1549.

Harley, M.D., Turner, I.L., 2008. A simple data transformation technique for pre-processing survey data at embayed beaches. Coastal Engineering 55 (1), 63–68.

Harley, M.D., Turner, I.L., Short, A.D., Ranasinghe, R., 2007a. Nearshore wave climate and localised erosion during storm events. 18th Australasian Coastal and Ocean Engineering Conference, no. 89 [published on CD], pp. 1–6.

Harley, M.D., Turner, I.L., Short, A.D., Ranasinghe, R., 2007b. Monitoring beach processes using conventional, RTK-GPS and image-derived survey methods: Narrabeen Beach, Australia. In: Woodroffe, C.D., Bruce, E.M., Puotinen, M., Furness, R.A. (Eds.), GIS for the Coastal Zone: A Selection of Papers from CoastGIS 2006. University of Wollongong, Australia, pp. 151–164.

Holland, K.T., Holman, R.A., Lippmann, T.C., Stanley, J., Plant, N.G., 1997. Practical use of video imagery in nearshore oceanographic field studies. IEEE Journal of Oceanic Engineering 22 (1), 81–92.

Holman, R.A., Stanley, J., 2007. The history and technical capabilities of Argus. Coastal Engineering 54 (6–7), 477–491.

Komar, P.D., 1998. Beach Processes and Sedimentation2nd ed. Prentice Hall, Inglewood Cliffs, New Jersey.

Kroon, A., Larson, M., Moller, I., Yokoki, H., Rozynski, G., Cox, J., Larroude, P., 2008. Statistical analysis of coastal morphological data sets over seasonal to decadal time scales. Coastal Engineering 55 (7–8), 581–600.

Kuriyama, Y., 2002. Medium-term bar behavior and associated sediment transport at Hasaki, Japan. Journal of Geophysical Research, Oceans 107 (C9), 12.

Kuriyama, Y., Ito, Y., Yanagishima, S., 2008. Medium-term variations of bar properties and their linkages with environmental factors at Hasaki, Japan. Marine Geology 248 (1–2), 1–10.

Lacey, E., Peck, J., 1998. Long-term beach profile variations along the south shore of Rhode Island, USA. Journal of Coastal Research 14 (4), 1255–1264.

Larson, M., Kraus, N.C., 1994. Temporal and spatial scales of beach profile change, Duck, North Carolina. Marine Geology 117 (1–4), 75–94.

Lippmann, T.C., Holman, R.A., 1990. The spatial and temporal variability of sandbar morphology. Journal of Geophysical Research, Oceans 95 (C7), 11575–11590.

List, J.H., Farris, A.S., 1999. Large-scale shoreline response to storms and fair weather. In: Kraus, N.C., McDougal, W.G. (Eds.), Coastal Sediments '99. Hauppauge, NY, pp. 1324–1338.

Lord, D., Kulmar, M., 2000. The 1974 storms revisited: 25 years experience in ocean wave measurement along the south-east Australian coast. In: Cox, R. (Ed.), International Coastal Engineering Conference. Sydney, pp. 559–572.

Mason, D.C., Davenport, I.J., Flather, R.A., 1997. Interpolation of an intertidal digital elevation model from heighted shorelines: a case study in the western Wash. Estuarine, Coastal and Shelf Science 45 (5), 599–612.

Masselink, G., Pattiaratchi, C.B., 2001. Seasonal changes in beach morphology along the sheltered coastline of Perth, Western Australia. Marine Geology 172 (3–4), 243–263.

McLean, R., Shen, J.S., 2006. From foreshore to foredune: foredune development over the last 30 years at Moruya Beach, New South Wales, Australia. Journal of Coastal Research 22 (1), 28–36.

Morton, R.A., Paine, J.G., Gibeaut, J.C., 1994. Stages and durations of post-storm beach recovery, southeastern Texas coast, USA. Journal of Coastal Research 10 (4), 884–908.

Nicholls, R., Wong, P., Burkett, V., Codignotto, J., Hay, J., McLean, R., Woodroffe, S.R.C., 2007. Coastal systems and low-lying areas. In: Parry, M., Canziani, O., Palutikof, J., Linden, P.V.D., Hanson, C. (Eds.), Climate Change 2007: Impacts, Adaptation and Vulnerability. Contribution of Working Group II to the Fourth Assessment Report of the Intergovernmental Panel on Climate Change. Cambridge University Press, Cambridge, U.K.

Nielsen, P., 1988. Wave setup — a field study. Journal of Geophysical Research, Oceans 93 (C12), 15643–15652.

Nielsen, P., Hanslow, D.J., 1991. Wave runup and distributions on natural beaches. Journal of Coastal Research 7 (4), 1139–1152.

Norcross, Z.M., Fletcher, C.H., Merrifield, M., 2002. Annual and interannual changes on a reef-fringed pocket beach: Kailua Bay, Hawaii. Marine Geology 190, 553–580.

Ojeda, E., Guillen, J., 2008. Shoreline dynamics and beach rotation of artificial embayed beaches. Marine Geology 253 (1–2), 51–62.

Phillips, J.D., 1986. Spatial-analysis of shoreline erosion, Delaware Bay, New-Jersey. Annals of the Association of American Geographers 76 (1), 50–62.

Plant, N.G., Holman, R.A., 1997. Intertidal beach profile estimation using video images. Marine Geology 140 (1–2), 1–24.

Plant, N.G., Holland, K.T., Puleo, J.A., 2002. Analysis of the scale of errors in nearshore bathymetric data. Marine Geology 191, 71–86.

Plant, N.G., Aarninkhof, S.G.J., Turner, I.L., Kingston, K.S., 2007. The performance of shoreline detection models applied to video imagery. Journal of Coastal Research 23 (3), 658–670.

Quartel, S., Kroon, A., Ruessink, B.G., 2008. Seasonal accretion and erosion patterns of a microtidal sandy beach. Marine Geology 250 (1–2), 19–33.
Ranasinghe, R., Callaghan, D., Stive, M.J.F., 2009. A process based approach to derive probabilistic estimates of coastal recession due to sea level rise. Proceedings of Coastal Dynamics 2009, Tokyo, Japan [published on CD].
Ranasinghe, R., McLoughlin, R., Short, A., Symonds, G., 2004. The Southern Oscillation Index, wave climate, and beach rotation. Marine Geology 204 (3–4), 273–287.
Rozynski, G., 2005. Long-term shoreline response of a nontidal, barred coast. Coastal Engineering 52 (1), 79–91.
Rozynski, G., Larson, M., Pruszak, Z., 2001. Forced and self-organized shoreline response for a beach in the southern Baltic Sea determined through singular spectrum analysis. Coastal Engineering 43 (1), 41–58.
Sallenger, A.H., Holman, R.A., Birkemeier, W.A., 1985. Storm-induced response of a nearshore-bar system. Marine Geology 64 (3–4), 237–257.
Sallenger, A.H., Krabill, W.B., Swift, R.N., Brock, J., List, J., Hansen, M., Holman, R.A., Manizade, S., Sontag, J., Meredith, A., Morgan, K., Yunkel, J.K., Frederick, E.B., Stockdon, H., 2003. Evaluation of airborne topographic lidar for quantifying beach changes. Journal of Coastal Research 19 (1), 125–133.
Shepard, F., 1950. Beach cycles in Southern California. Tech. rep., U.S. Army Corps of Engineers.
Short, A., 2007. Beaches of the New South Wales Coast2nd ed. Sydney University Press.
Short, A.D., Trembanis, A.C., 2004. Decadal scale patterns in beach oscillation and rotation Narrabeen Beach, Australia — time series, PCA and wavelet analysis. Journal of Coastal Research 20 (2), 523–532.
Siegle, E., Huntley, D.A., Davidson, M.A., 2007. Coupling video imaging and numerical modelling for the study of inlet morphodynamics. Marine Geology 236 (3–4), 143–163.
Swales, A., 2002. Geostatistical estimation of short-term changes in beach morphology and sand budget. Journal of Coastal Research 18 (2), 338–351.
Thom, B., Hall, W., 1991. Behaviour of beach profiles during accretion and erosion dominated periods. Earth Surface Processes and Landforms 16, 113–127.
Trenberth, K.E., 1984. Signal versus noise in the Southern Oscillation. Monthly Weather Review 112 (2), 326–332.
Turner, I.L., 2006. Discriminating modes of shoreline response to offshore-detached structures. Journal of Waterway, Port, Coastal and Ocean Engineering 132 (3), 180–191.
Turner, I.L., Aarninkhof, S.G.J., Holman, R.A., 2006. Coastal imaging applications and research in Australia. Journal of Coastal Research 22 (1), 37.
Uunk, L., Wijnber, K.M., Morelissen, R.M., 2010. Automated mapping of the intertidal beach bathymetry from video images. Coastal Engineering 57, 461–469.
Wijnberg, K.M., Terwindt, J.H.J., 1995. Extracting decadal morphological behaviour from high-resolution, long-term bathymetric surveys along the Holland coast using eigenfunction analysis. Marine Geology 126 (1–4), 301–330.
Wright, L.D., Short, A.D., 1984. Morphodynamic variability of surf zones and beaches — a synthesis. Marine Geology 56 (1–4), 93–118.
Zhang, K.Q., Douglas, B., Leatherman, S., 2002. Do storms cause long-term beach erosion along the U.S. East Barrier Coast? Journal of Geology 110 (4), 493–502.